The unexpected players: alkene-dipeptide bridges as mediators of vesicle adhesion

Martin Eduardo Villanueva, Jacobo Troncoso, Patricia Losada-Pérez, Aida Jover**

M. E. Villanueva, P. Losada-Pérez

Experimental Soft Matter and Thermal Physics (EST) Group, Department of Physics, Université libre de Bruxelles, Boulevard du Triomphe CP223, 1050 Brussels, Belgium

E-mail: patricia.maria.losada.perez@ulb.be

J. Troncoso

Instituto de Física e Ciencias Aeroespaciais, Departamento de Física aplicada, Universidade de Vigo, Campus As Lagoas, 32004 Ourense, Spain

A. Jover

Departamento de Química Física, Universidade de Santiago de Compostela, Facultade de Ciencias, Alfonso X o Sabio s/n, 27002 Lugo, Spain

E-mail: aida.jover@usc.es

Keywords: vesicles, lipids, peptides, alkenes, aggregation, adhesion

Abstract

Adhesion of lipid membranes is ubiquitous in many biological, biochemical and biophysical processes. It requires the membranes of apposing bilayers to be in very close proximity, overcoming electrostatic and hydration repulsion forces. Adhesion of lipid vesicles is an essential early step for fusion and involves the action of proteins leading to lipid mixing. When

no content mixing between vesicles occurs, adhesion can lead to aggregation, a useful phenomenon to form assemblies with interest in tissue mimics and functional biomaterials. However, it is not a straightforward process and it typically relies on vesicle functionalization by the use of complex linkers. In this work we report a very straightforward approach to induce aggregation in zwitterionic vesicles. We show the synergistic action of diphenylalanine, a small dipeptide, with amylene, an alkene customarily used as chloroform stabilizer, in inducing adhesion and aggregation of zwitterionic lipid vesicles. A combination of NMR spectroscopy, microscopy and thermodynamic characterization techniques is used to yield a detailed picture of the mechanisms by which the interplay between these small molecules affects bilayer organization, stability and adhesion.

1. Introduction

Phospholipid vesicles are typically used as surrogates for cell membranes in biophysical studies and as drug delivery systems and microreactors.[1–3] The interactions among them can result in their adhesion/aggregation and/or in their eventual fusion, adhesion being the initial contact step for two vesicles to fuse.[4] Aggregation and fusion are involved in many biological processes, the former being a hallmark of atherosclerosis,[5] ~~[5]~~ while the latter plays a vital role in neurotransmitter release and viral infection.[6,7] When used as membrane models, it is desirable for vesicles to be stable, while vesicle adhesion can be positive as precursor for fusion events, and aggregation to purposely segregate soluble membrane material, or beneficial to the release of entrapped drugs.[8] Experimental studies of these processes at a fundamental level resort to the use of artificial lipid membrane models, in the form of lipid vesicles or supported lipid bilayers (SLBs), systems whose lipid composition can be well-controlled.[9,10] The fabrication of lipid vesicles involves the dissolution of lipids in organic solvents as a first step.

Chloroform is the solvent generally used to dissolve the lipids, which are then dried forming a lipid film to be later hydrated with an aqueous buffer. Commercial chloroform has stabilizers, usually ethanol or a mixture of amylenes, to avoid degradation and the formation of phosgene, a very dangerous toxic compound.[11]

Aggregation of phospholipid vesicles can be described by DLVO (Derjaguin-Landau-Verwey-Overbee) and modified DLVO theories.[9,10,12] Vesicle stability is governed by the balance among electrostatic, van der Waals and hydration interactions. The aggregation of charged vesicles can be induced by the use of oppositely charged systems, by the addition of monovalent and divalent cations or by the change of buffer pH.[12–15] Electrostatic-driven aggregation of charged vesicles does not require the action of linkers, yet spontaneous disaggregation can take place quite fast due to lipid mixing of external monolayers upon adhesion, subsequent charge reversal and vesicle detachment.[13] In the case of uncharged membranes, aggregation is mainly impeded by the hydration repulsive force between the polar headgroups, and initial adhesion requires morphological changes in the vesicles.[13] Given the fact that van der Waals attraction is rather weak, adhesion agents or linkers are typically used to induce adhesion and aggregation in these systems. As a matter of fact, most agents consist of rather complex molecules or require vesicle functionalization.[4,16] Examples range from tethered DNA strands with complementary ends,[17] streptavidin-biotin binding[18] and polymers or polypeptides.[16,19,20] Spontaneous vesicle aggregation of zwitterionic vesicles by small molecules and peptides is, to our knowledge, poorly explored.

In this work we focus on the interplay and impact of short alkene and short peptides on the organization and eventual aggregation of model 1,2-dimyristoyl-sn-glycero-3-phosphocholine (DMPC) vesicles. We chose amylene, a completely apolar and widely used chloroform stabilizer and diphenylalanine (Phe-Phe), a dipeptide well-known for its ability to form hollow tubular assemblies, as well as for being the core motif for Alzheimer's β-amyloid peptide.[21]

In a recent report, we have shown that Phe-Phe (in the absence of amylene) interacts with DMPC bilayer in a concentration-dependent manner: at low concentrations it hardly affects bilayer organization, while increasing concentration promotes a mild weakening of membrane organization and stability. Phe-Phe likely locates at the DMPC headgroup-water interface and the probability of inserting in the membrane hydrophobic core increases with concentration.[22,23]

We use a combination of thermodynamic, nanomechanical, microscopy and spectroscopic techniques that provide complementary, multiscale information on lipid bilayer organization and related vesicle changes. Our results show significant differences in DMPC bilayer organization in the absence and presence of amylene stabilizer, as well as a clear tendency to vesicle adhesion and aggregation driven by the formation of intermembrane amylene and Phe-Phe complexes.

2. Results and Discussion

2.1. Monolayers at the air-water interface

The molecular organization of pure DMPC and Phe-Phe/DMPC mixtures containing either ethanol or amylenes as chloroform stabilizers was studied using Langmuir monolayer films. Surface pressure π *vs* area isotherms are depicted in **Figure 1a**. As shown by the black solid and dashed lines, DMPC displays its typical liquid-expanded (LE) phase over the entire compression isotherm, both for the amylenes and the ethanol-containing chloroform solutions. This indicates that neither the presence of ethanol nor amylenes (if any), are able to produce a significant effect on the interfacial organization of the saturated DMPC monolayer. Subsequently, two sets of samples composed of Phe-Phe/DMPC mixtures in the presence of ethanol or amylenes were studied. Significant changes on the molecular areas can be observed

between the isotherms of Phe-Phe/DMPC mixtures monolayers from ethanol-stabilized (dashed lines) and amylene-stabilized (solid lines) chloroform. Several repetitions of the samples at the different P/L ratios, dispersed in both solvents, allowed us to confirm that peptide/lipid mixtures in the presence of amylenes do experience a greater shift towards higher molecular areas than in the absence of this stabilizer. Thus, while the peptide is able to interact with DMPC membranes causing their expansion in both solvents, this effect is enhanced when amylene-stabilized chloroform was used. To better rationalize this trend, the limiting areas (A_{lim}; *i. e.,* the mean molecular area that would be covered by each lipid molecule at zero pressure) were extracted and included in **Table 1** for each of the tested samples. Thus, taking the difference between the area shifts for ethanol-stabilized and amylenes-stabilized samples (ΔA_{lim}) an average shift in molecular areas of about ~ 10 Å^2/molecule was systematically observed in all the cases.

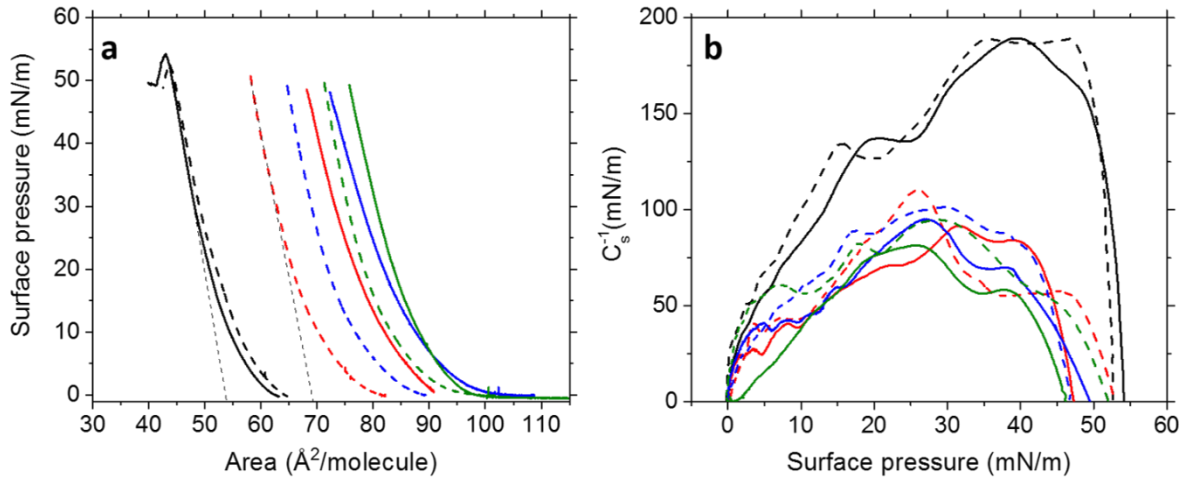

Figure 1. π-A isotherms (**a**) and variations in the surface compressional modulus (C_s^{-1}) with the surface pressure (**b**), for DMPC and Phe-Phe/DMPC in ethanol- (dashed lines) and amylenes- (solid lines) containing chloroform solutions. The colour code of the lines denoting the different P/L ratios is read as follows: pure lipid (P/L ratio=0, black), 0.05 (red), 0.1 (blue), and 0.2 (green). Exemplary extrapolating lines to π = 0 are drawn for the pure DMPC and P/L=

0.05 (amylenes containing) isotherms to show the estimated molecular limiting areas (A_{lim}). Experiments were carried out at T = 23 °C.

Table 1. Estimated limiting molecular areas (A_{lim}) and maximum compressibility modulus ($C_s^{-1}{}_{máx}$) for Phe-Phe/DMPC samples at the assayed P/L ratios.

	A_{lim} (Å^2/molecule)			$C_s^{-1}{}_{máx}$ (mN/m)		
P/L Ratio	EtOH	Amylene	ΔA_{lim}	EtOH	Amylene	$\Delta C_s^{-1}{}_{máx}$
0	55.3 ± 0.4	54.8 ± 0.2	-	189.3	189.2	-
0.05	69.1 ± 0.1	82.0 ± 0.5	12.9 ± 0.6	110.3	91.6	18.7
0.10	76.2 ± 0.4	88.1 ± 0.2	11.9 ± 0.6	101.5	95.0	6.5
0.20	81.7 ± 0.3	88.8 ± 0.4	7.1 ± 0.8	94.8	81.5	13.3

The surface compressional modulus, which reflects variations of the monolayer's in–plane elasticity, was calculated according to

$$C_s^{-1} = -A\left(\frac{d\pi}{dA}\right)_T , \qquad (1)$$

where C_s^{-1} is the reciprocal of the compressibility, and π is the surface pressure measured at each area point of the isotherm.[24] Variations in the compressional moduli *vs* π profiles can be directly linked to changes in the elastic properties of films. As shown in **Figure 1b**, DMPC lipid films experience a significant decrease in the C_s^{-1} at all the surface pressures, after the peptide incorporation. Extraction of the maximum compressibility modulus ($C_s^{-1}{}_{, max}$) from each of the obtained C_s^{-1} vs π profiles, enables a better comparison of the results (see **Table 1**). Similarly to what was observed from the area shifts, even the incorporation of a small amount of the peptide (P/L ratio= 0.05) is enough to produce an important decrease in the $C_s^{-1}{}_{, max}$ between 70−98 mN/m over the value of the pure DMPC. A further decrease in the $C_s^{-1}{}_{, max}$ values was obtained for all the samples containing amylenes. These differences are clear by the

$\Delta C_s^{-1}{}_{, max}$ quantities ($C_s^{-1}{}_{, max}^{EtOH}$- $C_s^{-1}{}_{, max}^{Amylene}$) which ranged from ~7 to 18 mN/m. This implies that amylenes would be able to associate and stabilize along the lipid-peptide joint at the air/water interface, enhancing the expansion effect of the peptide and furtherly increasing the fluidity of the lipid membrane, reverting in a more compressible surface.

So far, we were able to detect consistent differences between ethanol and amylenes-containing Phe-Phe/DMPC mixtures at the air-water interface. Controls on the pure solvents led to no interfacial activity, and given the poor adsorption and large uncertainty of Phe-Phe in all the solvents, only the mixture with the DMPC lipid were assayed to ensure repeatability (see Figure S1). Considering that the rest of the variables that could potentially play a role on the interfacial behaviour (i.e., concentration, temperature, subphase, spread volumes, etc.), were kept constant, this suggests that amylenes somehow help modulating the interaction between the peptide and the lipid as long as all the components are present the mixture.

2.2. Phase behavior of multilamellar vesicles in bulk and solid-supported

Bulk phase behavior multilamellar vesicles containing either DMPC or DMPC with Phe-Phe was assessed using calorimetry and densitometry. **Figure 2** highlights the differences obtained in melting temperatures, volumes, enthalpies, and width of the phase transition using both techniques for DMPC and Phe-Phe/DMPC mixtures formed in the presence of either ethanol or amylenes as chloroform stabilizers; large differences are noticeable. These latter show a much strong decrease of ΔT_m, Δh_m, and Δv_m against the P/L ratio, being it especially large for the transition enthalpy. Moreover, W_d strongly increases with the P/L ratio. All these results point towards the addition of diphenylalalnine induces a disordering of the lipid membrane structure making it more prone to be affected by temperature. Thus, the T_m decrease with the P/L ratio, and the difference between the volume and enthalpy of the ordered and disordered phase is smaller, showing the former to be more akin to the latter. Moreover, W_d, since it gives

information about the phase transition cooperativity −the lower the W_d, the higher the cooperativity is−, shows that it is decreased by the presence of diphenylalanine. The interplay of amylene and Phe-Phe seems to have an important role, weakening the membrane significantly. As a matter of fact, amylene or ethanol stabilizers do not change phase transition for pure DMPC (in the absence of Phe-Phe). Melting temperatures, enthalpies, volumes and width of the phase transition are, within the experimental uncertainty, the same, irrespective of the chloroform stabilizer when there is no diphenylalanine in the sample.

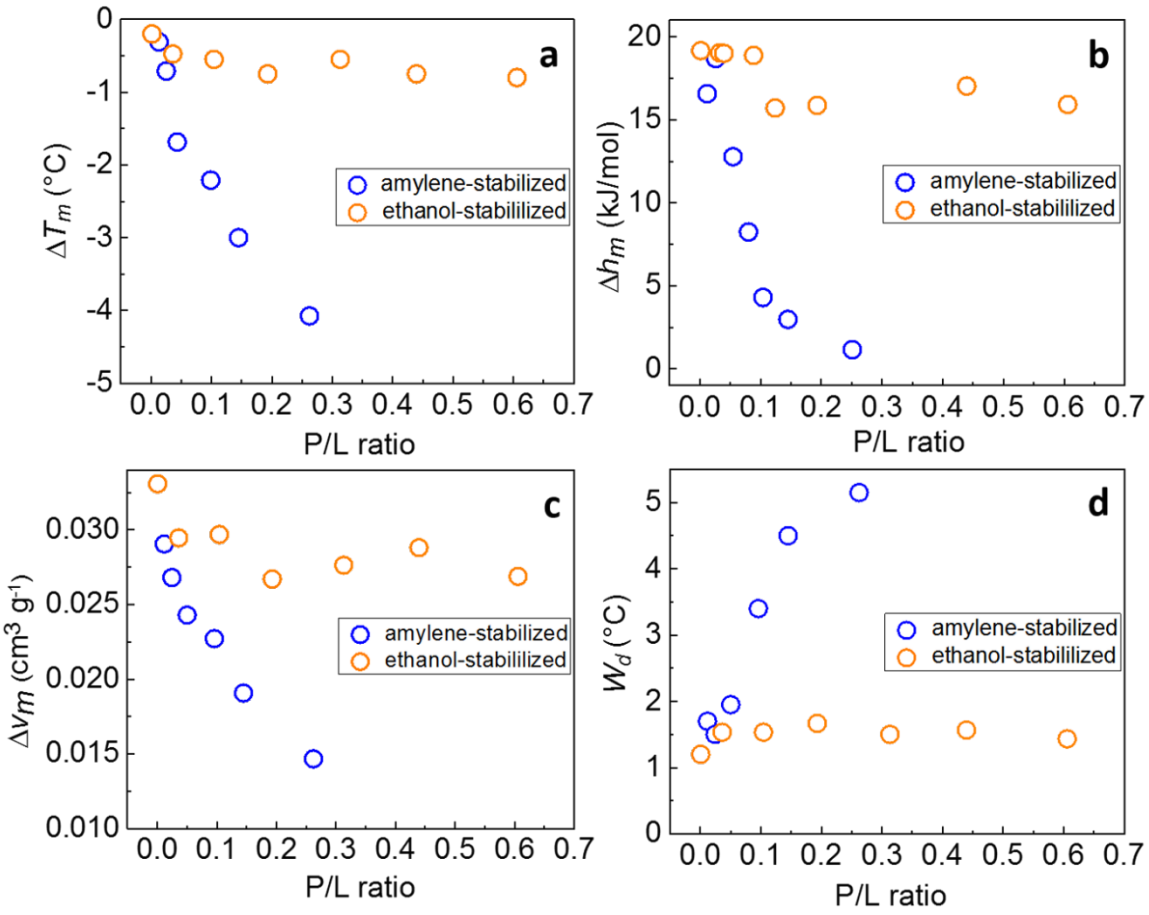

Figure 2. Phase transition properties in bulk for the studied systems against the P/L ratio. Orange- chloroform stabilized ethanol. Blue-chloroform stabilized with amylenes. From left to right and top to bottom: Shift in transition temperature ΔT_m, transition enthalpy Δh_m, transition volume Δv_m and width of the transition W_d.

Changes in the structural organization of the lipid molecules due to the incorporation of the Phe-Phe peptide were evaluated as well by assessing changes on the phase transition behavior of solid-supported vesicle layers. To this end, Phe-Phe/DMPC vesicle dispersions in MilliQ water were adsorbed onto Au-coated QCM-D sensors. **Figure 3** shows the phase transition profiles for the samples prepared in chloroform with ethanol (panel a) and chloroform with amylenes (panel b). As it can be observed, while some shift in the $T_{m,\,l}$ is obtained for samples from lipid films formed in ethanol-stabilized chloroform, lipid membranes formed in the presence of amylenes display much larger shifts of the phase transition peak towards lower temperatures at all the P/L ratios. Panels **c** and **d** show a comparison of the phase transition temperature shifts (ΔT_m) caused by the Phe-Phe peptide for both films prepared with and without amylenes, according to the P/L ratio. A general trend towards lower temperatures was obtained upon increasing P/L ratios, in agreement with the above-exposed results for samples in bulk, obtained from calorimetry and densitometry.

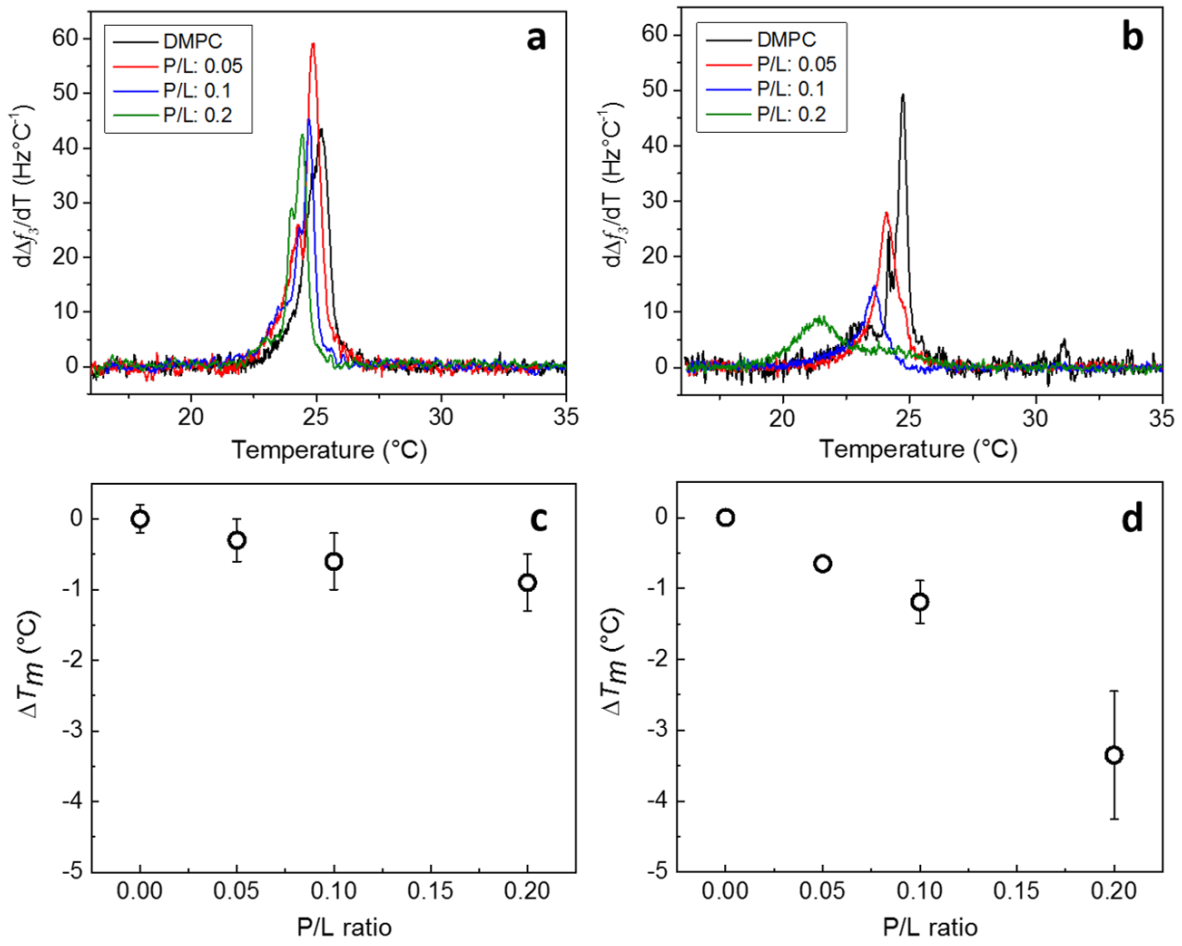

Figure 3. Phase transition profiles upon heating cycles of adsorbed DMPC and Phe-Phe/DMPC in MilliQ water, whose films were formed in CCl_3H-ethanol (**a**) and CCl_3H-amylenes (**b**); at all tested P/L ratios. In panels **c** and **d** are represented the respective temperature shifts (ΔT_m) induced by the presence of diphenylalanine in DMPC lipid bilayers. These data were extracted from the derivatives of the frequency changes observed by QCM-D upon heating the quartz sensors.

So far, the interaction between Phe-Phe and DMPC membranes was seen to be importantly modified in presence of remnant amylenes. It is worth stressing that the amylene content in the chloroform is very small (200 ppm) and traces should be (in principle) removed from the samples upon film drying and heating-water bath incubation (boiling point ~ 37.5-38.5 °C). In this regard, a possible scenario in which amylenes can associate with the pure peptide or form

part of a three-component interaction with the Phe-Phe/DMPC mixture could explain the permanence of the alkene impurities in the studied systems. With the aim to unveil the impact of the presence of amylenes on the nanomechanical and morphological properties of the lipid membranes, we proceeded to perform microscopy studies as follows in the next sections. Complementary insights on the amylenes concentration and differences with respect to the ethanol-stabilized samples acquired with ^{1}H-NMR, will allow us to understand the microscopic mechanism underlying the role of the alkene on the Phe-Phe/DMPC interaction.

2.3 Topographic and nanomechanical characterization by AFM

AFM was used to gain insights into the impact of Phe-Phe over SLBs formed from the rupture of vesicles fabricated with amylene-stabilized chloroform. SLBs of Phe-Phe/DMPC mixtures were formed onto ultraflat SiO_2 single crystal surfaces at different P/L ratios (from 0.05 to 0.2). **Figure 4** shows examples of AFM mapped areas for SLBs under study. As it can be observed, the larger the P/L ratio, the more defects (bilayer pores) on the DMPC lipid bilayers. These are indicated in Figure 4 by yellow arrows. As a matter of fact, at the largest P/L = 0.2 ratio, typical textures of membrane thinning effects can be observed, in agreement with previously reported effects on peptide thinning SLBs.[25] These results differ from previously reported measurements using ethanol-stabilized chloroform for preparing the peptide/lipid films, where almost no morphological changes were observed.[23]

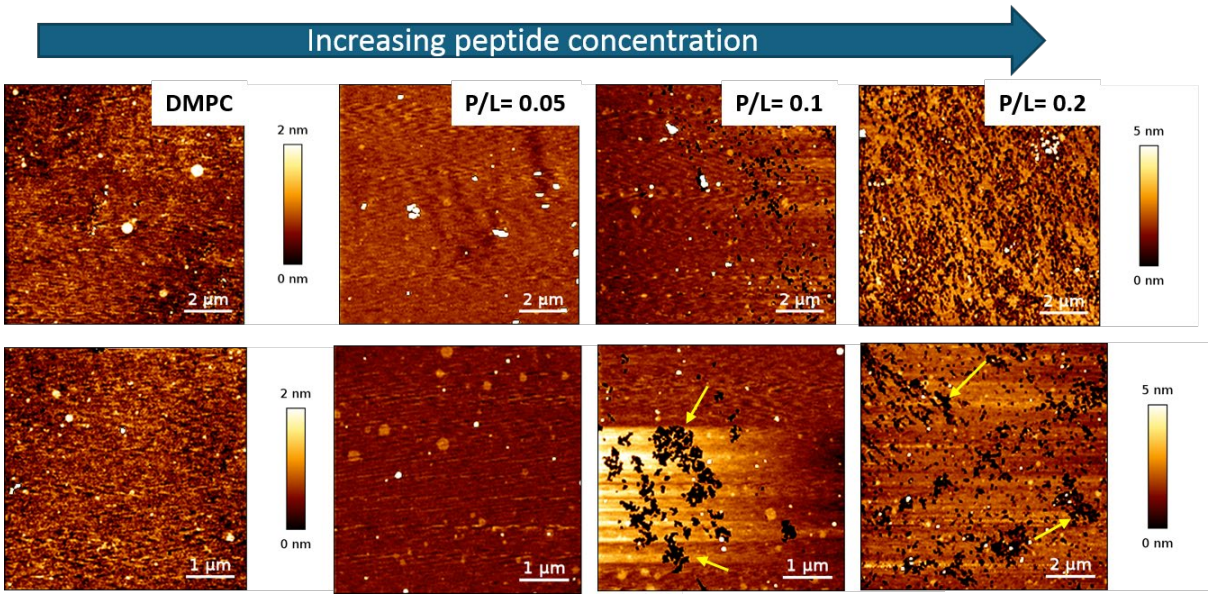

Figure 4. AFM quantitative images of DMPC, and Phe-Phe/DMPC at P/L ratios of 0.05, 0.1, and 0.2. QI-AFM imaging was performed in water onto mapping areas of 10 and 5 μm^2 avoiding any surface dewetting that could cause spontaneous hole formation or lipid aggregation. All the data were obtained with films prepared in amylenes-stabilized chloroform solutions. Experiments were carried out at T = 23 ºC. Bilayer pores are indicated by yellow arrows.

We then proceeded to perform dynamic force spectroscopy measurements on selected Phe-Phe/DMPC SLBs in order to assess their nanomechanical properties.[26] The penetration of the AFM tip through a SLB can be modelled as a two-state process: the tip on top of the bilayer and the tip in contact with the underlying solid surface. These states are separated by an energy barrier that is reduced by the application of an external force and that can be linked to the resistance to rupture of the SLB and thus the strength of lateral interactions between their constituent molecules.[27] By varying the tip-sample approach speed v and calculating the corresponding average breakthrough force F_b at each speed, it is possible to determine the probability of bilayer rupture that is directly related to the aforementioned energy barrier

involved in this process. The model that predicts the logarithmic dependence of F_b with the approach speed can be then fitted according to Equation 2 as:

$$F_b = a + b\log\frac{v}{v_0} \quad (2)$$

where F_b, a and b are in nN and v_0= 1μm/s. The fitting parameters a and b can then be used to evaluate the frequency at which a hole is spontaneously formed in the SLB, k_0, as:

$$k_0 = 1.596\frac{Kv_0}{b}10^{-\frac{a}{b}} \quad (3)$$

For testing on the probabilities of film rupture, Phe-Phe/DMPC films at 0.05 and 0.1 P/L molar ratios have been chosen. As depicted in **Figure 5**, both the systems follow an evolution towards higher breakthrough forces with increasing speed v. Calculations on the k_0 values yield $k_{0,\,P/L=0.05}$ = 24 ± 2 Hz, while for the SLB bearing the highest amount of peptide this parameter scaled to $k_{0,\,P/L=0.1}$ = 69 ± 3 Hz. These values are in line with those for classical phospholipids as reported by Costa *et. al*..[28] Changes in k_0 values are around the same magnitude as those obtained for SLBs exposed to pore-forming hydrophilic particles (i.e., with k_0 increasing between 3 and 5- fold respect to the pure lipid scenario.[29]

From these results, it can be concluded that the probability of pore formation increases with the amount of peptide that is present on the SLB formed from amylene-stabilized chloroform. This indicates that the bilayers loose nanomechanical stability and become less compact and more disordered, in agreement with results obtained from interfacial and thermodynamic characterization of monolayers and multilamellar vesicles, respectively.

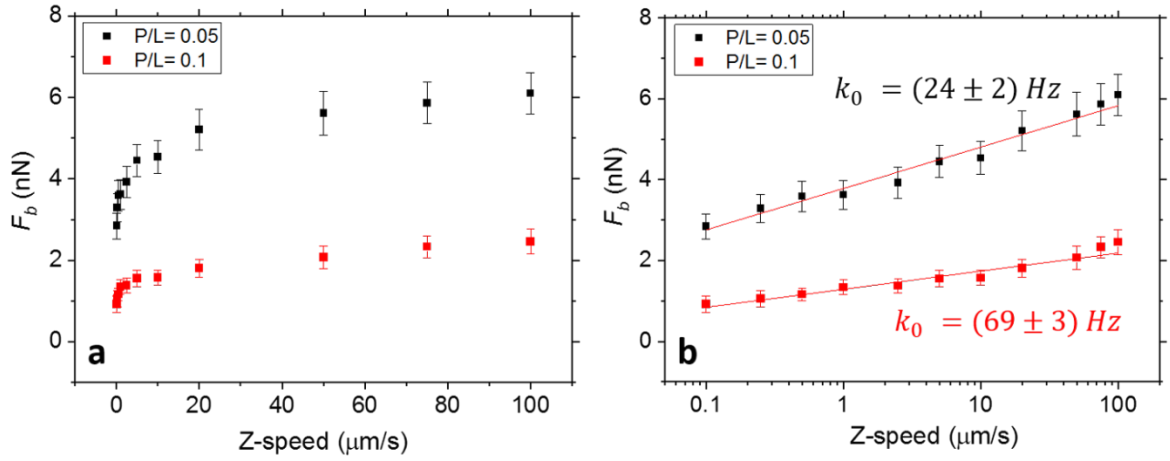

Figure 5. AFM-DFS (Dynamic Force Spectroscopy) performed on supported Phe-Phe/DMPC mixed bilayers formed on SiO_2 wafers. **a** Dependence of the tip approach speed on the breakthrough force values obtained for the 0.05 and 0.1 P/L ratios. **b** F_b vs tip approach speed in semi logarithmic scale along with the estimated values for the probability of rupture (k_0) for each SLB film. Experiments were carried out at $T = 23$ ºC.

To achieve a molecular picture as to understand the changes evidenced in the presence of amylene stabilizer via thermodynamic and AFM nanomechanical characterization, we conducted additional microscopy and NMR characterization of selected samples. We decided to keep the peptide to lipid ratio P/L=0.1 constant, and prepare different samples using small and large chloroform volumes (thus different concentration of amylene in the solvent). This way the lipid and peptide concentration are fixed, changing the amount of amylene present before the evaporation of the lipid film. **Table 2** provides an overview of all the samples studied by microscopy and NMR techniques. We use a code for referring the samples: Am and Et abbreviations specify the use of amylene or ethanol-stabilized chloroform. GV refer to samples prepared using the methodology described in point 2.1, with large volume of chloroform. A sample with no GV suffix indicates that the sample was prepared using a chloroform volume around twenty times smaller, implying a lower amylene concentration. The samples with low amylene concentration were also characterized using the other techniques. An intermediate

behavior, between ethanol and high amylene content samples were observed. Thus, no relevant insights could be extracted from these data and we decided to not include them for the sake of clarity.

Table 2. Description of the samples measured using microscopy and NMR. P/L= 0.1 for the samples with Phe-Phe. Amylene concentration in the chloroform solution, in mg per DMPC mg, are also given

	Description	Amylene concentration
DMPC-Am	Cl_3CH-amylene in small volume	0.035
PhDMPC-Et	Cl_3CH -EtOH	-
PhDMPC-Am	Cl_3CH-amylenes in small volume	0.035
PhDMPC-AmGV	Cl_3CH-amylenes in great volume	0.170
Ph-AmGV	Cl_3CH-amylenes in great volume	0.170
Ph-Am	Cl_3CH-amylenes in small volume	0.035

2.4. Microscopy of vesicles

To get a multiscale picture of the shape and size of vesicles in bulk, we performed Bright-Field Optical Microscopy (BFOM), Confocal Laser Scanning Microscopy (CLSM), and Transmission Electronic Microscopy (TEM). BFOM was carried out without staining or vesicle immobilization to avoid modifications in their behaviour and to observe the formed structures as they are in aqueous solution. Panels **a-c** in **Figure 6** display the micrographs of DMPC vesicles without Phe-Phe (panel a) and three samples containing vesicles DMPC/PhePhe mixtures at P/L = 0.1 prepared under different conditions. No significant dissimilarities in size distribution were observed among the samples, being all very polydisperse. However, while DMPC-Am and PhDMPC-Et samples consist of mainly isolated vesicles (panels **a** and **b**), PhDMPC-Am and PhDMPC-AmGV display mostly vesicles adhered to one another, indicating

that the combined presence of Phe-Phe and amylenes in the vesicle system induces aggregation, and becomes more evident with increasing amylene concentration.

Two fluorescent probes were used in confocal microscopy CLSM: rhodamine B, which interacts with the phospholipids membrane,[30] and Fast Green FCF, which associates to proteins.[31] Thus, they allow to disclose (globally) the distribution of the Phe-Phe dipeptide molecules in the DMPC bilayer structures.[32] Results are summarized in **Figure 6** (panels **e-l**) and reveal that Phe-Phe is located in the DMPC bilayer as FCF surrounds the vesicles (**Figure 6**, **j-l**). CLSM and BFOM images show consistent results, namely isolated vesicles in DMPC-Am and PhDMPC-Et samples and clear aggregation in PhDMPC-Am and PhDMPC-AmGV ones.

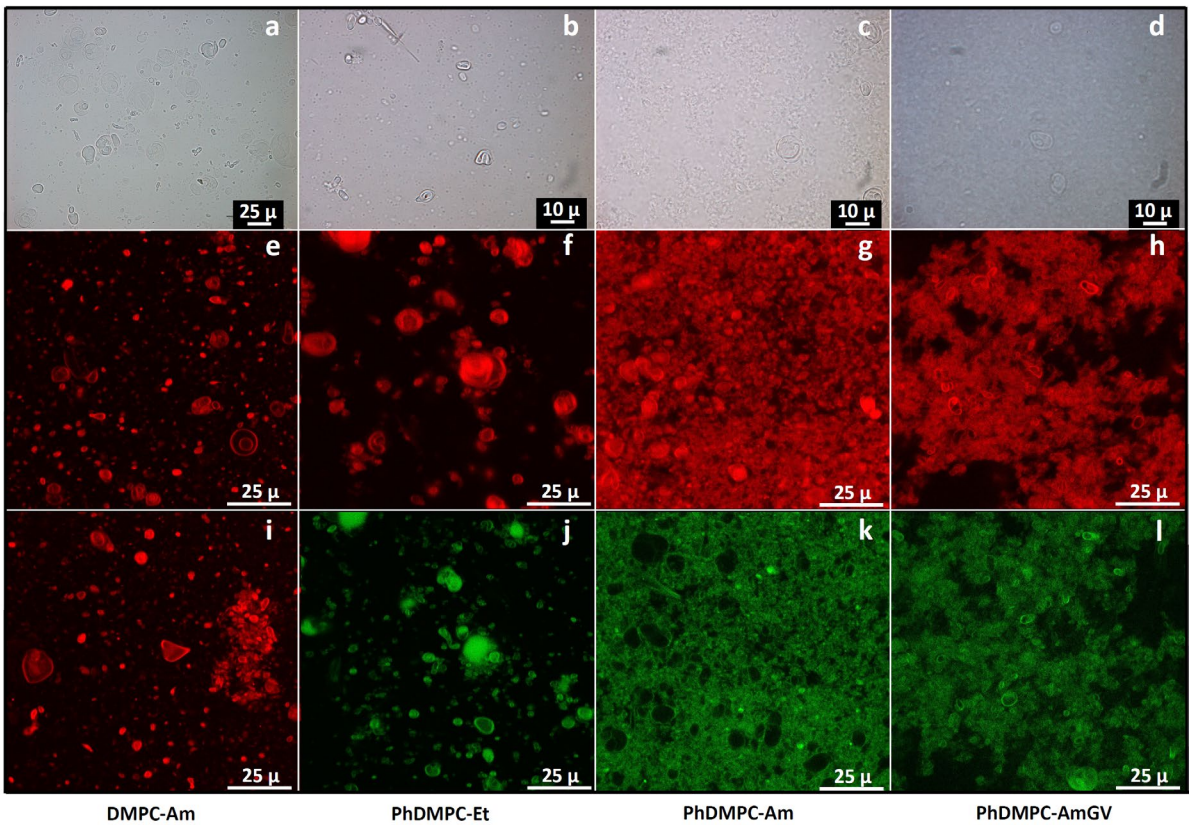

Figure 6. Bright Field Optical Micoscopy (BFOM, a-d) and Confocal Laser Scanning Microscopy (CLSM, e-l) images of DMPC-Am (a, e, i), PhDMPC-Et (b,f,j), PhDMPC-Am (c, g, k) and PhDMPC-AmGV (d, h, l). BFOM was performed without dyes inclusion and all the

CLSM images contain both Fast Green (green colour) FCF and Rhodamine B (red colour). No particle immobilization process was applied and experiments were carried out at $T = 20$ °C.

An additional picture of the vesicle structure and distribution at a smaller scale was obtained by TEM microscopy, where the vesicles have undergone a drying process before being introduced into the microscope.[33] This procedure could make the vesicles to change their shape and structure to some extent, unlike the other two microscopic techniques. TEM micrographs are displayed in **Figure 7** and show vesicles with a high degree of polydispersity. The TEM scale resolves the multilamellar structure of the vesicles (red arrows) in DMPC-Am, PhDMPC-Et, (smaller number of lamellae), and PhDMPC-Am, whereas unilamellar vesicles were observed for PhDMPC-AmGV. Small Phe-Phe fibers are also observed in all the samples containing Phe-Phe except in those of GV (parallel arrangement, green arrow in **Figure 7b**). This could be due to the saturation of peptide in the membrane structure. Therefore, the maximum Phe-Phe concentration is achieved, as a result of a dynamic equilibrium between the Phe-Phe placed in the membrane, in aqueous solution and in the crystalline form of fibers at P/L= 0.1. Vesicles at GV contain greater amylene concentration, which makes it to interact with the Phe-Phe (see next section) producing amylenes-(Phe-Phe) associations which avoid the fiber generation.

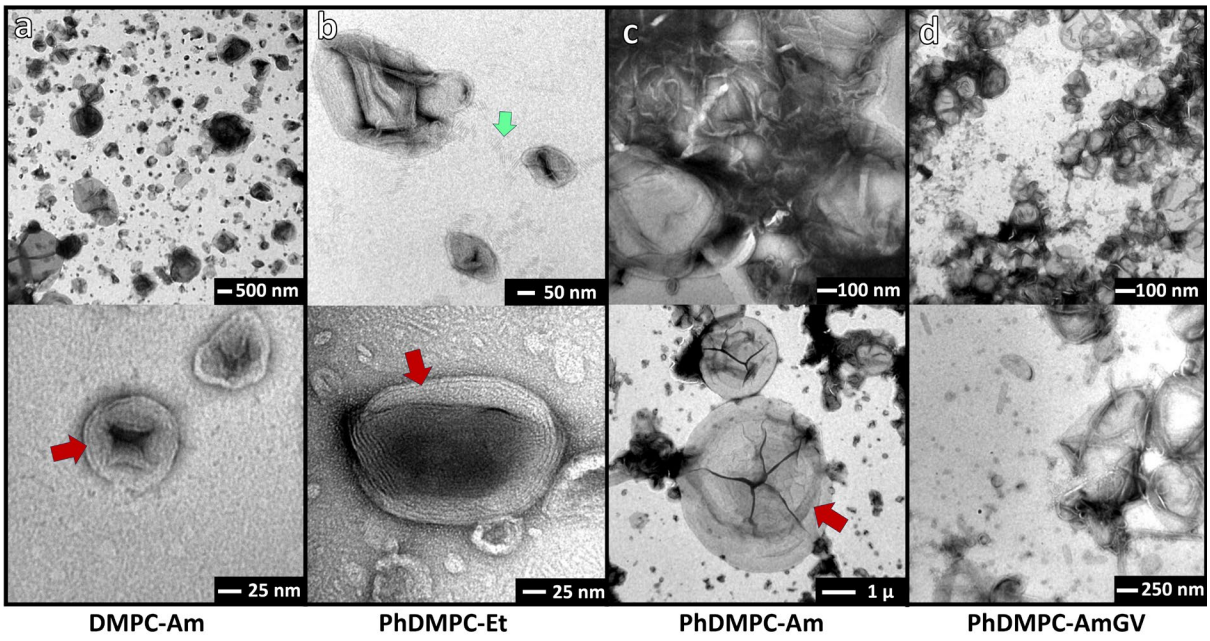

Figure 7. TEM images of vesicles: a) DMPC-Am, b) PhDMPC-Et, c) PhDMPC-Am and d) PhDMPC-AmGV. a-c display multilamellar vesicles (red arrows). Green arrow points out Phe-Phe fibers. Experiments were carried out at $T = 20$ °C.

2.5. Nuclear Magnetic Resonance

Figure 8 shows an overview of the NMR spectra of the samples under study. Spectra a and g show the results of pure DMPC dispersions; they almost completely lack of ^{1}H signals. This is nothing but a result of the self-assembly of DMPC molecules. They build up large multilamellar vesicles that greatly suppress the mobility of the phospholipid atoms within the timescale of the NMR experiments. Therefore, DMPC ^{1}H signals broaden and drastically decrease in intensity when compared to the ^{1}H signals of isolated DMPC molecules in solution (see Figure S2).[34,35] The only exception is the TMA peak at 3 ppm, visible at the highest temperature (arrow 2 in spectrum a), revealing that some motion is allowed due to the fluidity of the lipid membrane in these conditions. It is relevant to highlight the differences between these spectra and those in the literature with clearer signals, although broad and poorly defined, for all the DMPC hydrogens.[36,37] This is mostly due to vesicle dispersions previously reported were homogenized to uniform sizes (less than 200 nm) and/or were unilamellar.[37,38]

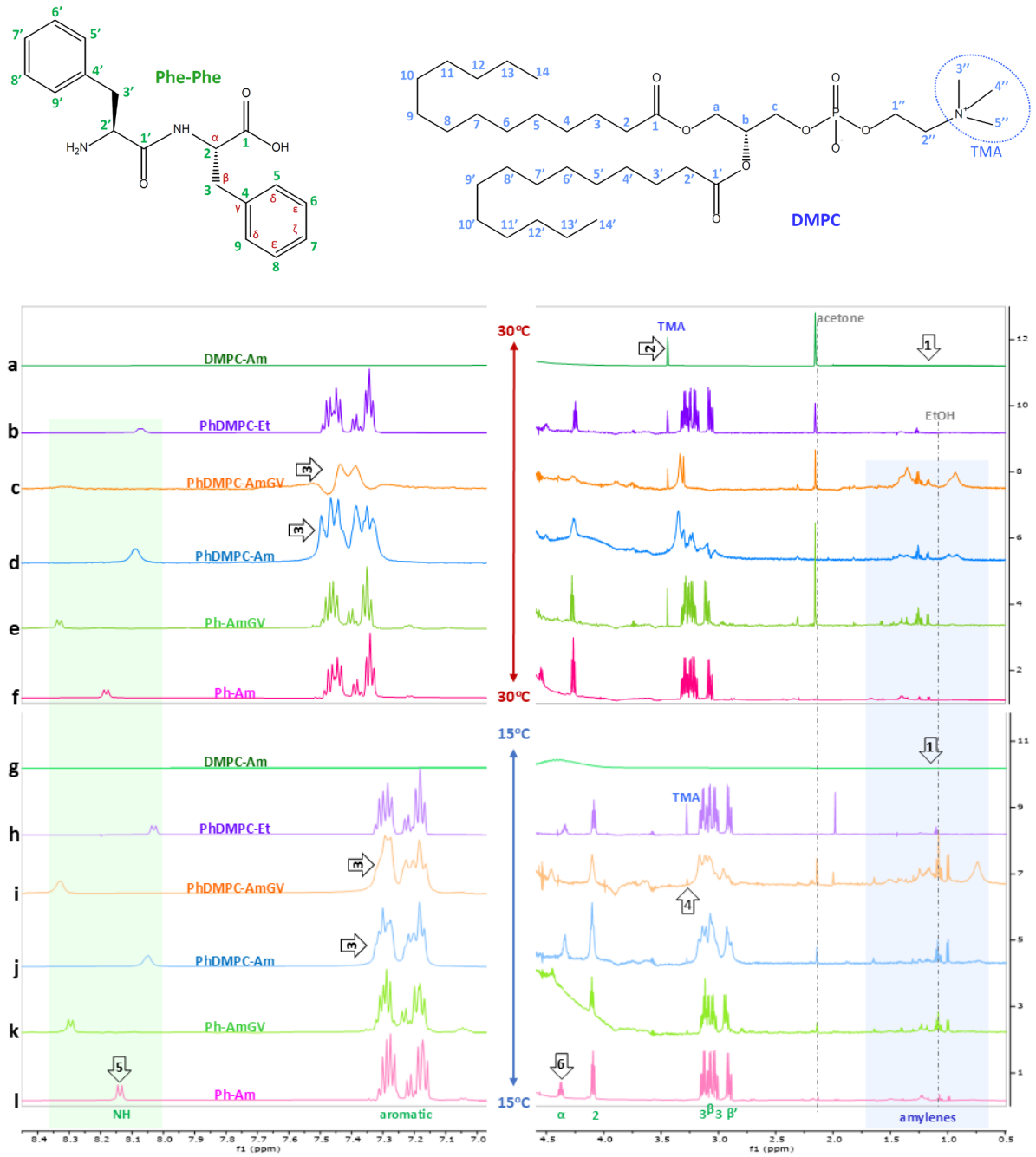

Figure 8. ^{1}H NMR spectra of a,g) DMPC-Am, b,h) PhDMPC-Et, c, i) PhDMPC-AmGV, d, j) PhDMPC-Am, e, k)Ph-AmGV and e, l) Ph-Am. Light colours correspond to T = 15 °C and dark colours to T=30 °C. Green labels correspond to Phe-Phe hydrogens, blue to DMPC, violet to amylene and grey labels indicate solvents. The samples were measured using a H_2O 95% D_2O 5% mixture as solvent. The green area represents the NH chemical shift range, and the blue area the main amylenes' range.

Another revealing feature observed in **Figure 8** is that the signal corresponding to amylene, indicated by the blue shadowed area of **Figure 8 c-f** and **h-l**,[39,40] are present only for the samples containing Phe-Phe. Therefore, amylene must bind to this peptide, forming supramolecular complexes and preventing it to be removed from the lipid cake during the solvent evaporation.

The different degree of widening and distortion for the NMR signals can easily visualized in **Figure 8**. The Phe-Phe signals for vesicles made with ethanol-stabilized chloroform (**Figures 8b and h)**; display a similar shape to the pure Phe-Phe dissolved in water (**Figure S3**). However, there is a strong distortion and widening of the diphenylalanine spectra for samples containing vesicles made using amylenes-stabilized chloroform (**spectra c, d, i, j**), especially visible for the aromatic rings and β hydrogens (chemical shifts around 7.15 ppm and 3 ppm at 15 ºC, respectively), facts associated with important restrictions over its movement. This indicates that most of diphenylalanine are in molecular configurations that strongly affect their mobility.

Chemical shifts in **Figure 8** can also give relevant information. All functional groups show important variations with temperature with the exception of NH. This suggests it is somewhat protected from the increase of the environmental polarity with temperature, probably due to the diphenylalanine - DMPC interaction through the diphenylalanine carboxylate (negative charge) and the TMA of DMPC (positive charge). In addition, the NH group is the only one that shows important differences between samples at the same temperature. Focusing on 15 ºC spectra, NH signal chemical shift is 7.90 ppm for diphenylalanine dissolved in water (see **Figure S3**), whereas it goes up to 8.03 ppm for the vesicles prepared using ethanol-stabilized chloroform (spectrum h), quite similar to that obtained for those prepared with the lowest amylene concentration (8.05 ppm, given in spectrum j). For pure diphenylalanine with the lowest amylene concentration (spectrum l), the NH chemical shift goes up to 8.14 ppm.

Therefore, amylene at low concentration has a small effect over NH when vesicles are present, but quite strong when they are not. If amylene concentration is raised, the NH shift goes up to 8.30 ppm for pure diphenylalanine (spectrum k) and up to 8.32 ppm if the sample contains vesicles (spectrum i). Thus, at high amylene concentrations, the above-observed tendency is reversed, and amylene affects more the NH when there are vesicles in the system.

These results together with those obtained with the other techniques can help to envisage a molecular model for the studied systems, depicted in **Figure 9**. The NMR data reveals that diphenylalanine make supramolecular complexes with amylene, which seemingly strongly affect the NH group. With a view on the molecular structure of both molecules, the only options are a diphenylalanine-amylene dimer (Figure 9a), a diphenylalanine-amylene-diphenylalanine trimer (**Figure 9b**), being the aromatic-amylene interaction in the origin of both supramolecular arrangements, and a diphenylalanine-amylene-amylene-diphenylalanine cyclic tetramer (**Figure 9c**). This latter configuration would facilitate the NH-carboxylate interaction in the diphenylalanine, and would be the cause of the strong NH chemical shifts observed at high amylene concentrations (arrow 1). It must be pointed out that more complex configurations would be possible, but they would be nothing but a combination of those above exposed.

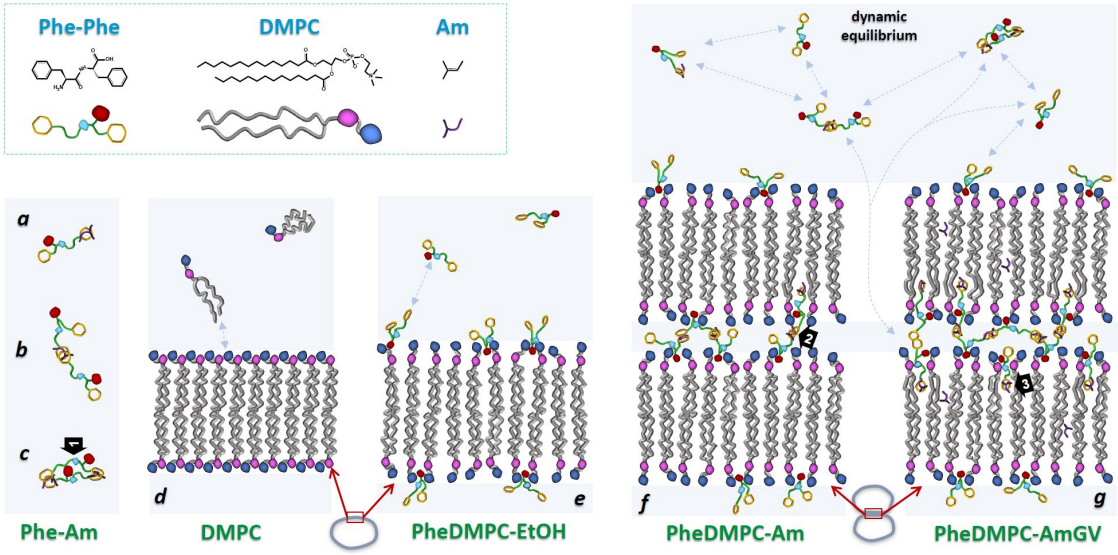

Figure 9. Molecular picture proposed for vesicle-peptide interaction that explains the experimental results. a-c) Amylene-diphenylalanine supramolecular complexes. d) Pure DMPC bilayer. e) DMPC bilayer formed in ethanol-stabilized chloroform with diphenylalanine. f) DMPC bilayer formed in amylene-stabilized chloroform with diphenylalanine at low amylene concentration. f) DMPC bilayer formed in amylene-stabilized chloroform with diphenylalanine at high amylene concentration. Red and turquoise blobs represent the carboxylate and NH group of diphenylalanine whereas pink and blue ones are the phosphate and trimethylamine groups of DMPC.

The diphenylalanine supramolecular complexes would be in dynamic chemical equilibrium that would be affected by the lipid membrane. Thus, at zero amylene concentration, there are no supramolecular complexes; in this case, diphenylalanine would be attached only to the membrane surface, through TMA-carboxylate bound (see **Figure 9e**). If amylene concentration is raised, the simpler complexes start to show up, acting as bridges between lipid bilayers, reverting in the observed vesicle adhesion (see **Figure 9f**). In both cases (zero or low amylene concentration), the NH group would interact with the DMPC phosphate, what would be at the

origin of the NH chemical shifts observed for PhDMPC-Et and PhDMPC-Am, and explains their similar values (8.03 vs. 8.05 ppm). The higher value of 8.14 ppm of the NH shift for PhDMPC-Am would be caused by the equilibrium displacement towards the tetramer or towards more complex supramolecular structures when the membrane is absent. In this case, DMPC would act as a competitive inhibitor of these complexes through the TMA, which binds the diphenylalanine carboxylate, and prevents the NH- carboxylate bounds between diphenylalanine molecules to be made. On the other hand, the widening and distortion of the NMR signals for PhDMPC-Am, as compared with PhDMPC-Et shows that diphenylalanine-amylene complexes are more prone to interact with the lipid membrane, being able to become part of the lipid fraction and to form bridges between adjacent vesicles, giving rise to vesicle adhesion (see **Figure 9f**, arrow 2).

If the amylene concentration goes further, the equilibrium between the diphenylalanine complexes goes towards the creation of larger supramolecular structures. This would increase the ratio of diphenylalanine in the lipid fraction, reverting in a high distortion of the NMR signals, increasing the adhesion between vesicles and weakening the membrane structure (see **Figure 9g**, arrow 3). In this context, it is worth to point out the high values obtained for the NH shift for PhDMPC-AmGV and Ph-AmGV (8.32 and 8.30 ppm), which would show that NH is located in a high polar environment, probably linked to the phosphate DMPC or to the carboxylate of other diphenylalanine that forms the supramolecular complex. In addition, these similar NH chemical shifts show that lipid membrane does not have influence over the equilibrium between the different diphenylalanine complexes at such large amylene concentrations, in contrast with the results obtained at low amylene concentration.

4. Conclusions

We have evaluated the impact of diphenylalanine on the integrity and adhesion of zwitterionic DMPC lipid vesicles prepared in the presence and absence of amylene chloroform stabilizers. Our approach consisted in a two-fold strategy: i) vesicles were prepared with a fixed amount of amylene and the concentration of diphenylalanine was increased, and ii) the concentration of diphenylalanine was fixed and vesicles were prepared using different amylene concentrations. The study of the peptide concentration dependence was carried out using thermodynamic and nanomechanical characterization. Significant differences in the DMPC lipid membrane lateral organization in the absence and presence of the amylene stabilizer were observed. Experiments with lipid monolayers showed that both the expansion (increase of the area per molecule) and film fluidization effects caused by the peptide are enhanced in the presence of amylenes. Similarly, the main phase transition of DMPC is shifted towards lower temperatures and becomes less cooperative with increasing peptide concentration, the changes being more pronounced in the presence of amylenes. Nanomechanical measurements by AFM dynamic force spectroscopy showed that bilayers display a weaker nanomechanical stability with increasing peptide concentration. AFM images revealed a membrane thinning effect in supported lipid bilayers formed at P/L ratio = 0.2 in the presence of amylene-stabilized chloroform. At the same P/L ratio no morphological changes in bilayers formed using ethanol-stabilized were observed.

Optical and TEM microscopies were employed to assess morphological changes in vesicles with a fixed P/L ratio of 0.1, a peptide concentration for which significant changes in lateral organization, phase transition and stability were observed as compared to pure DMPC bilayers. Microscopy images showed that samples without amylene consisted mostly of isolated vesicles, while an amylene-dependent vesicle aggregation effect was observed for vesicles containing diphenylalanine prepared in the presence of this alkene. It is worth mentioning that

aggregation was not observed for pure DMPC vesicles prepared in the presence of amylene stabilizer, indicating that amylenes alone do not induce vesicle adhesion if the peptide is not present.

A molecular model on vesicle adhesion and aggregation was provided by 1H-NMR measurements. In the absence of amylene, Phe-Phe peptide molecules interact with the outermost part of the membrane, locating at the headgroup aqueous interface and leading to mild bilayer disorder. Conversely, supramolecular bridges between amylene and Phe-Phe are formed in samples prepared with amylene-stabilized chloroform. The observed 1H-NMR shifts indicate that DMPC vesicle adhesion promoted by these bridges clearly depends on the amount of amylenes that are present in the mixture. While low amounts of the small alkene will induce vesicle adhesion by bridging bilayers of apposing membranes, high amylene concentrations allow the diphenylamine-amylene complexes to insert into the membrane's inner space, leading to a greater degree of disorder. Vesicles consisting of bilayers with higher degree of disorder are more prone to deform and will likely promote stronger adhesion (along a larger contact area), as observed by optical and TEM microscopy.

In summary, adhesion between zwitterionic vesicles can be straightforwardly achieved by a synergistic interaction of small alkenes and peptides. These results can serve as a reference for exploring other small molecules prone to display a similar combined effect, and pave the way towards programmable adhesion and aggregation by controlling the type and amount of adhesion agents.

2. Experimental Section

Sample preparation: DMPC lipid in powder form was purchased from Avanti Polar Lipids (Alabaster, AL) and di-L-phenylalanine from Sigma-Aldrich. Two chloroform types were used, one stabilized with 100-200 ppm of amylenes, with purity better than 0.995 in mass

fraction, and the other one stabilized with 0.4-0.6% of ethanol, with purity greater than 0.999 in mass fraction. The samples at the different P/L ratios were prepared both in ethanol- and amylene-stabilized chloroform as dispersant solvent for comparison. We found that the volume of ethanol-stabilized chloroform used for dissolving the powders is irrelevant, but this was not the case for the amylenes-stabilized one. Therefore, aliquots of a diphenylalanine chloroform solution at 0.13 mg/ml were added to the required volumes of DMPC chloroform solutions at 10 mg/ml in order to reach the P/L (peptide to lipid) weight ratios to be studied. The amount of amylene goes up to 0.35 mg per DMPC mg for the most concentrated diphenylalanine solutions. Some samples used in microscopy and NMR experiments were made using a protocol with lower chloroform volume, for the sake of comparison (see section 2.4). Multilamellar vesicles were subsequently prepared following previously reported standard procedures [23] . P/L mixed films were formed by drying the mixed components in the organic solvent with a gentle N_2 stream and 48 h vacuum. Then, the films were hydrated in Milli-Q water to form stock solutions at 2 mg/mL (QCM-D and AFM) and 10 mg/mL (density and heat capacity experiments) under continuous stirring for 45 min, in a temperature-controlled water bath at 40 °C. Dilutions of the above-mentioned stock solutions were properly made to reach the final working concentrations depending on the performed technique and experiments.

Langmuir isotherms: The Langmuir films of DMPC and Phe-Phe/DMPC mixtures were obtained by spreading an aliquot of each corresponding sample at the air-water interface of a Langmuir trough, with a Hamilton microsyringe (precise to ± 0.25 μL). All the solutions were prepared both in ethanol- and amylene-stabilized chloroform. Phe-Phe/DMPC mixtures at 0.05, 0.1, and 0.2 P/L ratios were obtained by mixing proper volumes of the respective stock solutions. The total number of molecules in mixed monolayers (5×10^{16}) was kept constant in all the experiments. The surface pressure-area (π–A) isotherms were obtained in Milli-Q water on a KSV 2000 Langmuir balance (KSV, Helsinki, Finland) equipped with a Wilhelmy-type

pressure measuring system. The film compression (using a barrier speed of 10 mm/min) was initiated 5 min after spreading to ensure total evaporation of the solvent. The temperature of the aqueous subphase was held constant at (23 ± 1) °C with a Lauda E200 circulating water bath (Lauda Königshofen, Germany). The absence of surface-active impurities in the spreading solvent and aqueous subphase was routinely checked before each run as reported elsewhere.[41] At least three π *vs A* isotherms were measured and averaged. Reproducibility was within a maximum standard error of the mean of 1 mN/m for the surface pressure and under 1% of the mean area.

Vibrating tube densitometry: The density of multilamellar vesicles was measured using a high precision DMA5000 densimeter (Anton Paar, Austria). Temperature ramps were carried out upon heating with a step of 0.1 °C. From raw density data, three relevant quantities can be calculated, namely the bulk transition temperature T_m, the width of the transition W_d, and the volume change during the transition between gel and fluid phases. T_m can be determined by identifying the peak in the derivative of the density versus temperature curves. From this curve, the width of the transition peak W_d, a quantity representative of the degree of the cooperativity in the phase change, can also be determined. The change in volume upon the transition, Δv_m is obtained through the calculation of the specific volume, v_s, using the formula:

$$v_s = \frac{1}{c}\left(\frac{1}{\rho_d} - \frac{1-c}{\rho_s}\right) \quad (1)$$

where ρ_d and ρ_s are the density of the solution and solvent, respectively, and c is the concentration of the lipid in weight fraction. v_s was fitted against temperature to a straight line well above and below the phase transition, and the transition volume is calculated as the height between the two lines at the transition temperature. Uncertainties in T_m, W_d, and Δv_m, were estimated in 0.3 C, 0.4 °C, and 0.004 $cm^3 \cdot g^{-1}$, respectively. Details about the calculation procedure and experimental methodology are given elsewhere in refs.[23] and [42].

Differential scanning calorimetry: Calvet differential scanning calorimetry was used to determine T_m and enthalpy Δh_m of the gel-fluid phase transition. Temperature ramps of 0.25 °C·min^{-1} were used in all the experiments. Calibration was carried out using dry air and water, their heat capacity values being obtained from [43]. The reference cell was filled with water in all experiments. T_m was obtained from maximum of the peak of the heat capacity versus temperature curves, whereas the transition heat was determined by integrating the heat capacity peak after substracting the baseline. Uncertainties in T_m, W_d, and Δh_m, were estimated in 0.3 °C and 3 kJ·mol^{-1}, respectively. The reported bulk T_m value was estimated to be the mean value of those obtained from calorimetry and densitometry. A more detailed explanation of this methodology is given in [23].

Quartz crystal microbalance with dissipation monitoring (QCM-D): An Qsense E4 instrument (Biolin Scientific, Sweden) measuring frequency and dissipation changes for different odd overtones, Δf/n and ΔD (with n, the overtone number) has been used. AT-cut quartz crystals with Au coating (diameter 14 mm, thickness 0.3 mm, quoted surface roughness < 2 nm, and resonant frequency 4.95 MHz) were employed. The Au-coated quartz sensors were cleaned for 5 minutes with a 5:1:1 mixture of Milli-Q water, ammonia and hydrogen peroxide heated at 70 °C, UV-ozone treated with a UV-ozone cleaner (Bioforce Nanosciences, Germany) for 15 min, rinsed in Milli-Q water and dried with N_2. The changes in Δf/n andΔD were monitored at five different overtones (from 3rd to 11th). The lipid vesicles were injected into the QCM-D cells with a flow rate of 50 µl/min. Vesicle adsorption onto the Au-coated sensors was carried out at 16 °C, the temperature stability at constant temperature being in the order of ± 0.02 °C. A baseline with Milli-Q water was first established and lipid vesicles were injected afterwards over the Au-coated sensor chips. After reaching a stable supported vesicle layer the pump was switched off and the ensemble was left to stabilize for 30 minutes. Heating scans from 16 to 35 °C were then performed at a rate of 0.4 °C/min. Usually, phase transitions are characterized

by a finite jump in both frequency and dissipation temperature dependent signals.[44,45] Their temperature derivative thus yields extrema, providing a straightforward way for determining the onset and completion temperatures of the transition.

Contact angle measurements: Contact angle (CA) measurements were carried out using an Attension ThetaLite from Biolin Scientific (Sweden) based on the sessile drop method in order to determine the wettability of Au-coated surfaces used during QCM-D experiments. A 3 μL drop of Milli-Q water was dispensed onto clean, UV-ozone treated Au-coated sensor, and the shape of the drop formed on the surface was analysed. The average of all contact angles measured for each Au-coated surfaces was estimated to be 28 ± 5 °.

Atomic force microscopy with force spectroscopy: Supported lipid bilayers (SLBs) were formed by incubating for 15 minutes DMPC or Phe-Phe/DMPC vesicle suspensions onto very flat SiO_2 at 45 °C inside an INCU-Line® 68R incubator (VWR chemicals, Leuven Belgium). Prior to the AFM measurements, the SiO_2 surfaces were rinsed with buffer avoiding SLB dewetting. AFM imaging and nanomechanical measurements were performed using a JPK Nanowizard 4 BIO-AFM from Bruker (Nano GmbH, Berlin, Germany). All the measurements were performed in milli-Q water at room temperature in an AFM fluid cell. Triangular silicon nitride MLCT-E cantilevers (Bruker, Nano GmbH, Berlin, Germany) with quoted cantilever length of L ~ 140 μm, resonance frequency f ~ 38 kHz, nominal spring constant k ~ 0.1 N/m and nominal tip radius of 20 nm were used. The AFM cantilever was calibrated in Milli-Q water against a clean glass slide according to the thermal noise method.[46] QI images (using Quantitative imaging mode) were recorded at different scan sizes using a pixel sampling of 256 × 256, cantilever speed of 45 μm/s, and setpoint force of 300 pN. In order to assess the nanomechanics of the SLBs in the presence and absence of the peptide, both static and dynamic force spectroscopy was carried out. In order to assess and compare the nanomechanical properties of Phe-Phe/DMPC SLBs prepared from lipid films with and without amylenes, force maps

over square grids with 16 × 16 points were performed, with a force curve recorded per point. For each sample, several square grids were performed in different regions of the surface to assess the homogeneity of the results. A force setpoint of 10 nN and approach speed of 1 μm/s were used. Force spectroscopy measurements were carried out at the same temperature as AFM imaging (T = 25 °C). Dynamic force spectroscopy AFM measurements were also performed at different tip approach velocities and, as it will be shown in the results section, with setpoint forces between 10 and 20 nN. The AFM images were analysed using the JPK Data Processing software®, where the micrographs were flattened using the appropriate lowest order of levelling for each image.

Bright-Field Optical Microscopy (BFOM): Multilamellar vesicles for bright field optical microscopy were maintained under 15 °C and resuspended with a Pasteur pipette. A drop was deposited on a slide together with a coverslip. The samples were observed in a Nikon E800 optical microscope at different magnifications depending on the size of the vesicles, using dry objective lenses of 10x and 20x for the larger sizes and immersion objective lenses of 40x, 60x and 100x for the smaller vesicles. A Nikon DS-U2 digital camera assisted by the NIS-Elements D 2.30 SP1 software was used to acquire the images.

Confocal Laser Scanning Microscopy (CLSM): Fluorescent dyes Fast Green FCF (ThermoFisher >95.0%, λexcitation = 635 nm and λemission = 650-710 nm) and Rhodamine B (Sigma-Aldrich ≥95%, λexcitation = 532 nm and λemission = 600-700 nm) were used since they bound to diphenyalanine and DMPC, respectively. Samples were mixed with both fluorescent dyes a few minutes before the measurement in a final concentration of 5μg/ml Fast Green FCF and 2.5 μg/ml Rhodamine B. A Leica TCS SPE confocal microscope (Leica Microsystems GmbH, 35578 Wetzlar Germany), equipped with three solid-state lasers with wavelengths 488 nm, 532 nm and 635 nm was used to obtain digital images with 1024 x 1024 pixels resolution.

Transmision Electronic Microscopy (TEM): Multilamellar vesicles samples were resuspended until the liquid appears uniformly white and cloudy with a micropipette and a 2.5 μL drop was deposited on Formvar/Carbon supported copper grids with 400 mesh size. The samples are not sufficiently electron-dense to get sharp images, so uranyl acetate was added to the solution, widely used in TEM to observe the phospholipid membranes.[47] Specifically, a drop of 2% aqueous uranyl acetate was deposited on top of the sample for 30 seconds, the excess removed with a Whatman filter and let dry. The samples were examined on a JEOL JEM-1400 Flash (80 kV) (JEOL, Japan) equipped with a JEOL EM-14661 FLASH camera assisted by the TEM Center Ver.1.7.20 software.

Nuclear Magnetic Resonance (NMR): 1H NMR spectra and Bidimensional COSY and ROESY experiments were recorded on a Bruker AVANCE DPX600 (600 MHz) and on a Bruker AVANCE DPX400 (400 MHz) spectrometers at 15 and 30 °C, selected to characterize the gel and fluid phases, respectively. Chemical shifts are reported in ppm from tetramethylsilane (TMS) with the solvent resonance as the internal standard (water 95% D_2O 5%, 4.79 ppm).

Supporting Information

Supporting Information is available from the Wiley Online Library or from the author.

Acknowledgements

Support from the Spanish Ministry of Science, Innovation, and Universities under Grants No. PID2020-115722GB-C22 and PID2023-147148NB-I00 are greatly acknowledged. Support from the project ‘DELTA’ with project number 40008129 by ‘Fonds de la Recherche

Scientifique' (FNRS). A. J. would also acknowledge A. López Greco for his help in the model discussion.

References

[1] Y. Lu, G. Allegri, J. Huskens, *Mater. horizons* **2022**, *9*, 892.

[2] L. van der Koog, T. B. Gandek, A. Nagelkerke, *Adv. Healthc. Mater.* **2022**, *11*, DOI 10.1002/adhm.202100639.

[3] V. Noireaux, A. Libchaber, *Proc. Natl. Acad. Sci. U. S. A.* **2004**, *101*, 17669.

[4] C. M. Paleos, D. Tsiourvas, Z. Sideratou, *ChemBioChem* **2011**, *12*, 510.

[5] K. Oorni, M. O. Pentikainen, M. Ala-Korpela, P. T. Kovanen, *J. Lipid Res.* **2000**, *41*, 1703.

[6] J. Rizo, C. Rosenmund, *Nat. Struct. Mol. Biol.* **2008**, *15*, 665.

[7] S. C. Harrison, *Nat. Struct. Mol. Biol.* **2008**, *15*, 690.

[8] X. Guo, F. C. Szoka, *Acc. Chem. Res.* **2003**, *36*, 335.

[9] B. V. Derjaguin, L. Landau, *Acta Physicochim. U.R.S.S.* **1941**, *14*, 633.

[10] J. N. Israelachvili, *Intermolecular and Surface Forces*, Academic Press, Santa Barbara, **2011**.

[11] G. M. Dyson, *Chem. Rev.* **1927**, *4*, 109.

[12] S. Ohki, H. Ohshima, *Colloids Surfaces B Biointerfaces* **1999**, *14*, 27.

[13] D. Saeki, S. Sugiura, T. Baba, T. Kanamori, S. Sato, S. Mukataka, S. Ichikawa, *J. Colloid Interface Sci.* **2008**, *320*, 611.

[14] H. Minami, I. Tohru, S. Ryosuke, *J. Colloid Interface Sci.* **1993**, *158*, 460.

[15] K. Suzuki, K. Kurihara, Y. Okura, T. Toyota, T. Sugawara, *Chem. Lett.* **2012**, *41*, 1084.

[16] N. De Lange, F. A. M. Leermakers, J. M. Kleijn, *Soft Matter* **2020**, *16*, 2379.

[17] L. Parolini, B. M. Mognetti, J. Kotar, E. Eiser, P. Cicuta, L. Di Michele, *Nat. Commun.* **2015**, *6*, 6948.

[18] S. Chiruvolu, S. Walker, J. Israelachvili, F. Schmitt, D. Leckband, J. A. Zasadzinski, *Science (80-.).* **1994**, *264*, 1753.

[19] T. Janas, K. Nowotarski, T. Janas, *Chem. Phys. Lipids* **2010**, *163*, 286.

[20] I. Plasencia, L. Rivas, K. M. W. Keough, D. Marsh, J. Pérez-Gil, *Biochem. J.* **2004**,

377, 183.

[21] C. H. Görbitz, *Chem. Commun.* **2006**, 2332.

[22] B. B. Gerbelli, E. R. Da Silva, B. Miranda Soares, W. A. Alves, E. Andreoli De Oliveira, *Langmuir* **2018**, *34*, 2171.

[23] L. Bar, P. Losada-Pérez, J. Troncoso, *J. Mol. Liq.* **2023**, *384*, 122196.

[24] J. T. Davies, E. K. Rideal, *Interfacial Phenomena*, Academic Press, London, **1963**.

[25] K. Hammond, M. G. Ryadnov, B. W. Hoogenboom, *Biochim. Biophys. Acta - Biomembr.* **2021**, *1863*, 183447.

[26] L. Redondo-Morata, P. Losada-Pérez, M. I. Giannotti, in *Curr. Top. Membr.*, **2020**, pp. 1–55.

[27] H. J. Butt, V. Franz, *Phys. Rev. E - Stat. Physics, Plasmas, Fluids, Relat. Interdiscip. Top.* **2002**, *66*, 1.

[28] O. Saavedra V., T. F. D. Fernandes, P. E. Milhiet, L. Costa, *Langmuir* **2020**, *36*, 5709.

[29] M. E. Villanueva, L. Bar, L. Porcar, Y. Gerelli, P. Losada-Pérez, *J. Colloid Interface Sci.* **2025**, *677*, 620.

[30] N. Magalhães, G. M. Simões, C. Ramos, J. Samelo, A. C. Oliveira, H. A. L. Filipe, J. P. P. Ramalho, M. J. Moreno, L. M. S. Loura, *Molecules* **2022**, *27*, 1420.

[31] C. M. Wilson, *Anal. Biochem.* **1979**, *96*, 263.

[32] S. Gallier, D. Gragson, R. Jiménez-Flores, D. Everett, *J. Agric. Food Chem.* **2010**, *58*, 4250.

[33] N. Koifman, Y. Talmon, *Pharmaceutics* **2021**, *13*, DOI 10.3390/pharmaceutics13071015.

[34] R. J. Gillams, J. V. Busto, S. Busch, F. M. Goñi, C. D. Lorenz, S. E. McLain, *J. Phys. Chem. B* **2015**, *119*, 128.

[35] M. Delcea, S. Moreno-Flores, D. Pum, U. B. Sleytr, J. L. Toca-Herrera, *On the Lipid-Bacterial Protein Interaction Studied by Quartz Crystal Microbalance with Dissipation, Transmission Electron Microscopy and Atomic Force Microscopy. Http://Arxiv.Org/Abs/0904.1662*, **2009**.

[36] G. Da Costa, L. Mouret, S. Chevance, E. Le Rumeur, A. Bondon, *Eur. Biophys. J.* **2007**, *36*, 933.

[37] C. Schwieger, A. Achilles, S. Scholz, J. Rüger, K. Bacia, K. Saalwaechter, J. Kressler, A. Blume, *Soft Matter* **2014**, *10*, 6147.

[38] S. V. Dvinskikh, V. Castro, D. Sandström, *Phys. Chem. Chem. Phys.* **2005**, *7*, 607.

[39] Z. Zhang, T. Xiao, H. Al-Megren, S. A. Aldrees, M. Al-Kinany, V. L. Kuznetsov, M.

L. Kuznetsov, P. P. Edwards, *Chem. Commun.* **2017**, *53*, 4026.

[40] V. Bellière, C. Lorentz, C. Geantet, Y. Yoshimura, D. Laurenti, M. Vrinat, *Appl. Catal. B Environ.* **2006**, *64*, 254.

[41] M. E. Villanueva, A. E. Lanterna, R. V. Vico, *J. Colloid Interface Sci.* **2019**, *543*, 247.

[42] D. Fitzgerald, C. Du, S. Asaph, *Technical Assessment of the Anton Paar DMA5000 Density Meter*, United Kindom, **2000**.

[43] E. W. Lemmon, M. O. McLinden, D. G. Friend, in *NIST Chem. WebBook, NIST Stand. Ref. Database Number 69* (Eds: P.J. Linstrom, W.G. Mallard), National Institute Of Standards And Technology, Gaithersburg MD, 20899, USA, **1998**.

[44] S. K. Pramanik, S. Seneca, A. Ethirajan, S. Neupane, F. U. Renner, P. Losada-Pérez, *Biointerphases* **2016**, *11*, 019006.

[45] S. Neupane, Y. De Smet, F. U. Renner, P. Losada-Pérez, *Front. Mater.* **2018**, *5*, 1.

[46] E. L. Florin, M. Rief, H. Lehmann, M. Ludwig, C. Dornmair, V. T. Moy, H. E. Gaub, *Biosens. Bioelectron.* **1995**, *10*, 895.

[47] J. Asadi, S. Ferguson, H. Raja, C. Hacker, P. Marius, R. Ward, C. Pliotas, J. Naismith, J. Lucocq, *Micron* **2017**, *99*, 40.

ToC

M. E. Villanueva, J. Troncoso, P. Losada-Pérez*, A. Jover*

The unexpected players: alkene-dipeptide bridges as mediators of vesicle adhesion

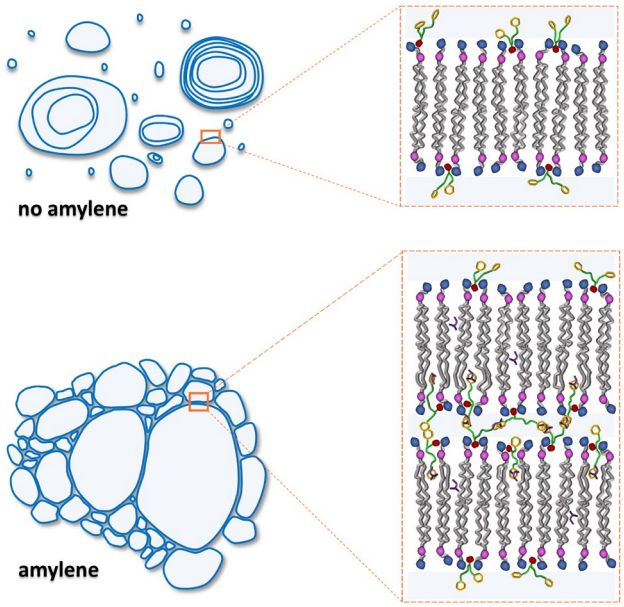

Phospholipids are commonly used as in vitro models for cellular membranes. When combined with diphenylalanine and amylenes, they promote complete adhesion between membrane vesicles, preserving their vesicular integrity and modifying their strength and thermodynamic properties. A phenyl-amylene-phenyl bridge appears to be the key factor responsible for this effect.